Research Article

Simulation of surface flux received through breast tumor radiation therapy with MCNPX code

P. Afshin [a], Sh. Shahi [a, b, *] and F. Azimifar [a]

a Department of Biomedical Engineering, Isfahan (Khorasgan) Branch, Islamic Azad University, Isfahan, Iran.
b Laser and Biophotonics in Biotechnologies Research Center, Isfahan (Khorasgan) Branch, Islamic Azad University, Isfahan, Iran.

*** Corresponding Author Email : shahilaser@khuisf.ac.ir**

DOI: 10.30495/ijbbe.2023.1992892.1030

ABSTRAC

Received: Aug. 2, 2023, Revised: Aug. 27, 2023, Accepted: Oct. 17, 2023, Available Online: Oct. 18, 2023

In radiation therapy, investigating the effects of the surface flux reaching the tissue is important in planning the treatment and this requires a precise evaluation of the absorbed dose distribution throughout the irradiated tissue. Therefore, the Monte Carlo simulation with MCNP code was designed. A point source with the size of E, a spectrum width of 0.6 µm, a single energy transfer of 6 MeV to the breast tumor tissue, a size of 2 × 4 × 4 $cm^{3,}$ and also a density (Kg/$\boldsymbol{m^3}$) of 11.34 at a fixed depth of 3 cm is radiated from a standard phantom (VIP MAN) made of tissue. The results show the highest surface flux that received on the tumor is around 9.97 × $\mathbf{10^{-6}}$ $\frac{N}{Cm^2 s}$ *and is located almost in the center of the tumor in dimensions (-0.75 cm - 1.3 cm). The lower surface flux around the tumor is caused by the rate of the dose that is distributed. Also, the template phenomenon in the creation of electrons is based on the Compton effect, while in the creation of photons, the Compton effect did not occur.*

KEYWORDS

Radiotherapy, Absorbed dose distribution, Breast tumor, Surface flux, Code MCNPX.

I. INTRODUCTION

Today, radiation therapy is a common way to treat cancer. In radiation therapy, the main goal is to deliver the highest dose of radiation to the treated volume (tumor) with the lowest dose in the surrounding organs and tissues. However, during treatment, the incoming or scattered radiation may pass through the non-target organs and tissues, which is considered an undesirable dose in the treatment process [1]. Therefore, selective and targeted drug delivery is a very promising strategy to overcome the various issues caused by random distribution of drugs, such as serious side effects and receiving an effective dose higher than expected in the treatment protocol. Therefore, selective targeting of specific tissues or cells, especially around the tumor sites, is of particular importance [2].

Modern medical devices in clinical radiotherapy work with artificial intelligence-based methods [3], [4], and Monte Carlo (MC) simulation with MCNPX code is used to analyze their data. This code is in good agreement with experimental results in various studies, especially in the investigation of proton beams on specific thicknesses such as neck organs, and it works very powerfully for radiation transfer simulation [5]-[7].

As it is not easy to directly measure the effects of radiation on various human tissues during radiation therapy, various models of human computational phantoms have been designed for using in Monte Carlo radiative transfer codes in different age groups for both male and female genders since the 1950s. At first, the investigations were limited to parts of the body tissue such as the human head, but little by little these phantoms were developed over time, and in 1960, Fisher and Snyder were able to design the entire human body with a phantom called MIRD in a comprehensive and close to reality [8]. In 2000, a phantom named VIP MAN was designed with more than 7.3 billion voxels, which allows extremely fine and color image analysis [9].

In radiation therapy, the dose calculation algorithms are used in treatment planning to calculate the delivered dose distribution to target volumes and organs at risk. Therefore, accurate dose calculations are required so that clinicians can reliably cover target volumes and achieve the best performance in sparing adjacent organs and soft tissues. Monte Carlo algorithms can provide accurate modeling of dose calculation by simulating the delivery and interaction of many particles with calculations based on particle simulation and providing the highest accuracy through the definition of patient geometry, which will lead to reliable clinical decisions. There is also a deep learning-based denoising capability for simulated MC dose distributions with a large number of particles [10].

The energy delivered to the tissue and the dose absorbed by the tissue is of particular importance for radiotherapy and imaging applications [11]. In radiation therapy, treatment planning requires an accurate assessment of the absorbed dose distribution throughout the target organs and tissues. It includes a wide range of radiotherapy approaches such as the use of photons, electrons, protons, carbon beams, and radioisotopes with different beam transfer conditions such as wide beam, rotating beam, brachytherapy, and targeted radionuclide therapy. In diagnostic imaging applications involving ionizing radiation, such as Computed Tomography, Positron Emission Tomography: (PET), and Single Photon Emission Tomography: (SPECT).

Assessment of the absorbed dose is important for a better analysis of the risks and merits of this method. In new methods, imaging and treatment are increasingly intertwined. Cone-beam imaging is associated with conventional LINAC radiation therapy, the CT is performed during tomotherapy, radiographic pairs are acquired during Cyberknife treatments, and new imaging systems are being developed for treatment monitoring in hadrontherapy [12].

In this article, the breast tissue is considered as the target tissue of radiation therapy, inside a standard tissue phantom to investigate the effects of surface flux (Flux) reaching the tissue for a fixed depth of the tissue and a fixed initial beam energy.

II. MATERIALS AND METHODS

In this research, Monte Carlo simulation with MCNPX code has been used to perform calculations, which has high statistical accuracy and its main purpose is to investigate the transport of various particles. In this code, the data related to the particle collision cross sections, the interaction between particles, as well as the photon interaction with elements from atomic number z = 1 to z = 100 are available by default, but to run the code specifically and for each specific project. The geometry of the problem includes the set of cell cards and the surface card, then physical parameters such as springs are defined, the appropriate sequence is applied to calculate the desired parameters, and finally, the program is executed.

At first, breast tumor fat tissue with the size of $2\times4\times4$ cm^3 and density (Kg/m^3) of 11.34 at a depth of 3 cm from a standard phantom (VIP MAN) is considered. The E-sized point source with a spectrum width of 0.6 μm is located at a distance of 77 cm from the surface of the tissue perpendicular to the tissue. The source radiation

will be sent to the tumor with a single energy transport of 6 MeV and after passing through a collimator that will adapt the cross-section of the beam field to the cross-section of the tumor. This collimator is located at a distance of 67 cm from the surface of the tissue, and its opening is considered to be square (similar to the surface of the target tissue), with sides of 1.5 cm^2 = 0.75 cm × 0.75 cm (1). The collimator aperture and the depth of the target tissue are adjusted to each other. Cartesian Tally mesh is used to calculate the dose. Therefore, the target tissue and its surrounding area are divided into meshes with dimensions of 2×2×2 mm^3 in three dimensions of x, y, and z.

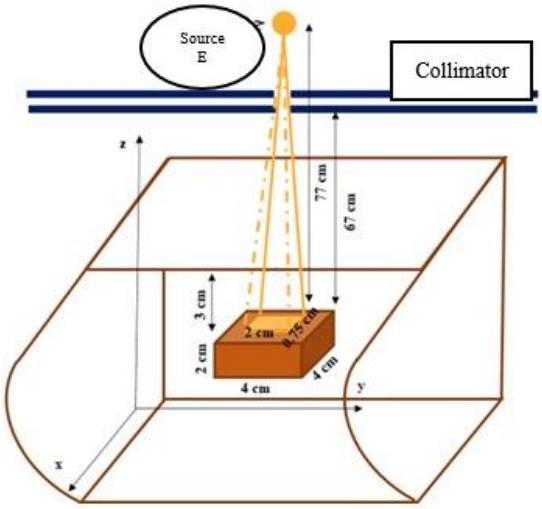

Fig. 1 Schematic image of the breast tissue and phantom under the radiation of the E-point source beam with a width of 0.6 µm.

III. RESULT AND DISCUSSION

The data from a one-month case file of female breast cancer patients of Omid Hospital in Isfahan, who were exposed to X-ray radiation from a LINAC machine, were used in this research. To simulate this device, an electron source as a point source with 6 MeV energy a Gaussian distribution with FWHM = 10 cm, and a Gaussian transverse profile with FWHM = 3 cm were considered as the radial profile of the dose at the depth of 3 cm of the phantom. The surface flux reached different points of the phantom (hypothetical tumor) and the energy distribution of the X-ray produced 6 MeV energy.

The surface flux data reached the selected tissue from the MCNPX code in Table 1 shows that the highest surface flux of 9.97 x 10^{-6} and the lowest surface flux of 1.05 x 10^{-6} reached the tumor in dimensions (0.75 cm - 1.3 cm) and dimensions (3.8 cm - 1.5 cm), respectively. Because the radiation from the point source leads to the non-uniformity of the surface flux reaching the tissue. Therefore, the received surface flux in the center of the tumor is higher than in the corners. For these surface flux values, the error rate obtained through the code is 0.44. Figure 2 shows the simulated image of these data.

In this image, the red point corresponds to the highest surface flux and the dark blue point shown by the arrow is the lowest surface flux that reached the tumor. In addition, the more energy the beam has lost, the more cells it has destroyed, which is indicated by the color spectrum from pale blue to green with the highest contribution.

The result of implementing the rmesh command (Cartesian or rectangular mesh), meshing from -4 cm to +4 cm, and dividing it into 40 equal parts, leads to providing a file called mdata. This file has a series of unintelligible sentences, whose data has been made meaningful using the GridConv program, and its output can be seen in Figure 3 of the amount of surface flux reaching the texture with meshing.

Table 1 Comparison of surface flux in the distribution of tumor tissue in different dimensions and fixed depth 3 cm.

Tumor) x (cm) (width	Tumor) y (cm) (length	Surface Flux
2.7	0.9	6.98E-06
-1.1	1.3	1.18E-06
-2.5	1.5	2.25E-06
-1.3	-0.75	9.97E-06
0.5	1.9	2.00E-06
-1.1	2.1	2.15E-06
1.3	2.3	2.13E-06
-1.5	2.7	6.47E-06

-2.3	3.1	1.18E-06
-0.1	3.3	2.46E-06
-1.5	3.5	4.19E-06
-2.3	3.7	2.15E-06
-1.5	3.8	1.05E-06

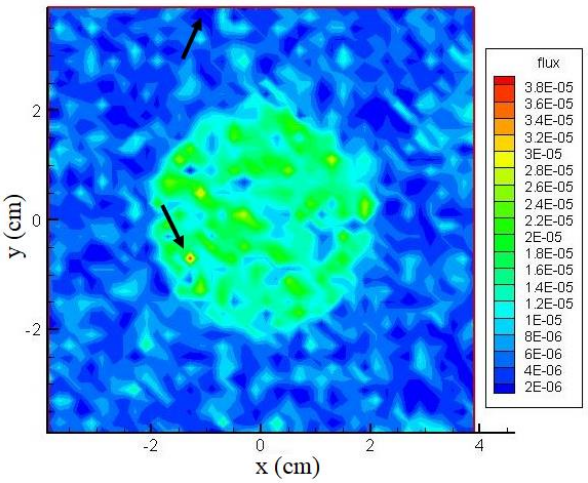

Fig. 2 Simulation of the amount of surface flux reaching the breast tissue at a depth of 3 cm in two dimensions

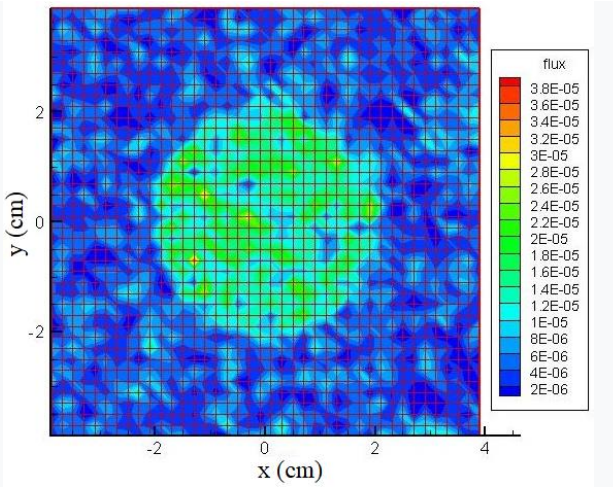

Fig. 3 The meshed image of the surface flux reaching the breast cancer tissue phantom at a depth of 3 cm with an energy of 6 MeV.

On the other hand, when X-rays are produced by a device obtained from another Thali, both photons and electrons are produced as can be seen in Tables 2 and 3. The data in Table 2 shows that after tracking photon and electron particles one million times, the Bremsstrahlung effect occurred 1821 times in photon creation and P-annihilation occurred 260 times. Also, according to the data of this table, in the process of photon loss, escape 976357 times and pair production 17495 times are the dominant phenomena, and phenomena such as Compton recoil and photonuclear occur.

Table 2 Creation and loss of photons in breast tissue at a depth of 3 cm

energy	weight	tracks	photon creation
6.00E+00	1.00E+00	1000000	source
0	0	0	nucl. interaction
0	0	0	particle decay
0	0	0	weight window
0	0	0	cell importance
0	0	0	weight cutoff
0	0	0	energy importance
0	0	0	dxtran
0	0	0	forced collisions
0	0	0	exp. transform
0	0	0	from neutrons
7.98E-05	1.82E-03	1821	bremsstrahlung
1.33E-04	2.60E-04	260	p-annihilation
0	0	0	photonuclear
0	0	0	electron x-rays
0	0	0	1st fluorescence
0	0	0	2nd fluorescence
0	0	0	(gamma,xgamma)
0	0	0	tabular sampling
6.00E+00	1.00E+00	1002081	total

energy	weight	tracks	photon loss
5.83E+00	9.76E-01	976357	escape
1.47E-07	1.16E-03	1160	energy cutoff
0	0	0	time cutoff
0	0	0	weight window
0	0	0	cell importance
0	0	0	weight cutoff
0	0	0	energy importance
0	0	0	dxtran
0	0	0	forced collisions
0	0	0	exp. transform
5.72E-02	0	0	Compton scatter
6.87E-03	7.07E-03	7069	capture
1.03E-01	1.75E-02	17495	pair production
		0	photonuclear abs
6.00E+00	1.00E+00	1002081	total

Although such phenomena are observed in Table 3 which is related to the phenomenon of electron creation, the escape phenomenon is much reduced compared to the state of photon creation. In addition, the dominant phenomena in creating electrons are knock-on and Compton, respectively. Therefore, the amount of radiation energy, sex, dimensions, and depth of the tumor all affect the data output.

Table 3 Creation and loss of electrons in breast tissue at a depth of 3 cm

energy	weight	tracks	Electron creation
0	0	0	source
0	0	0	nucl. interaction
0	0	0	particle decay
0	0	0	weight window
0	0	0	cell importance
0	0	0	weight cutoff
0	0	0	energy importance
6.54E-04	2.80E-04	280	pair production
4.29E-03	3.23E-03	3227	Compton recoil
6.73E-06	4.97E-04	497	photo-electric
0	0	0	photon auger
0	0	0	electron auger
1.80E-03	3.35E-01	334580	knock-on
0	0	0	(gamma,xelectron)
6.75E-03	3.39E-01	338584	total

energy	weight	tracks	Electron loss
2.64E-04	1.14E-04	114	escape
3.31E-04	3.38E-01	338470	energy cutoff
0	0	0	time cutoff
0	0	0	weight window
0	0	0	cell importance
0	0	0	weight cutoff
0	0	0	energy importance
0	0	0	scattering
0	0	0	bremsstrahlung
0	0	0	interact or decay
6.75E-03	3.39E-01	338584	total

In this simulation, it is predicted that 1002081 photons and 333584 electrons were created and lost from the total irradiation of 1000000 beams with 6 MeV energy to the tumor, after passing through the tumor, and the increase of 2081 photons in the tumor indicates the occurrence of chain reactions.

In the continuation of the data obtained from the code, it is possible to mention the capability of the MCNP code in simulating the impact of the particle on the target tissue, and the investigation of the impact of the particles in the number of different intercepted the particles obtained has been collected in Table 4.

Table 4 The efficiency of particle estimation reached by the system at a depth of 3 cm.

The number of particles intercepted	collisions	block	miss
6000000	100%	0%	100
7000000	100%	0%	100
8000000	100%	0%	100
9000000	99%	1%	100
10000000	99%	1%	0%
11000000	99%	1%	0%
12000000	99%	1%	0%

The results obtained from the number of particles captured by the code can be seen in different intervals. As can be seen from the results obtained from the number of intercepted particles performed by the code in different intervals, the higher the number of intercepted particles, the more accurate the error becomes, and on the other hand, it is determined at 6 MeV energy. How much is the error about the particle reaching the boundary texture? Another discussion obtained from the MCNP code looked at the weight balance of an electron in the target tissue, what happens to an electron from the time it enters the tissue to the time it leaves, and its brief description is for two intervals of 6 million interceptions. We report the particle and 12 million times of particle interception in two tables 5 and 6 below.

Table 5 Balance weight of an electron after 6 million times of random events at a depth of 3 cm.

External events			
total	inside the tumor	On the tumor	cell index
1.8000E-05	1.0167E-05	7.8333E-06	entering
0	0	0	source
-3.363E-01	-3.340E-01	-2.236E-03	energy cutoff
0	0	0	time cutoff

-1.468E-04	-1.366E-04	-1.016E-05	exiting
Physical events			
2.5267E-04	2.5133E-04	1.3333E-06	pair production
3.3553E-03	3.3370E-03	1.8333E-05	Compton recoil
4.8750E-04	4.8483E-04	2.6667E-06	photo-electric
0	0	0	photon auger
3.3333E-07	0	3.3333E-07	electron auger
3.3234E-01	3.3013E-01	2.2158E-03	knock-on
0	0	0	nucl. interaction
0	0	0	particle decay

Table 6 Balance weight of a photon after 12 million times of random occurrence at a depth of 3 cm.

External events			
total	inside the tumor	On the tumor	cell index
1.9182E-05	1.0636E-05	8.5455E-06	entering
0	0	0	source
-3.380E-01	-3.357E-01	-2.330E-03	energy cutoff
0	0	0	time cutoff
-1.435E-04	-1.329E-04	-1.063E-05	exiting
Physical events			
2.5782E-04	2.5636E-04	1.4545E-06	pair production
3.4429E-03	3.4256E-03	1.7273E-05	compton recoil
4.9455E-04	4.9191E-04	2.6364E-06	photo-electric
0	0	0	photon auger
3.6364E-07	0	3.6364E-07	electron auger
3.3400E-01	3.3169E-01	2.3106E-03	knock-on
0	0	0	nucl. interaction
0	0	0	particle decay

From the results obtained in Tables 5 and 6 for the cellular index, it can be understood that due to the tracking, the tracking of particles has doubled, but the results obtained regarding the inside of the tumor and the total events around and inside the tissue are very similar and many particles can be intercepted, but a certain number in this energy range have the ability to enter the tissue. The important Compton effect occurs near 3.35, which is based on discussing the energy by repeating the simulation and intercepting more particles. It has been a process that helps us a lot in designing better treatments for patients.

IV. CONCLUSION

The MCNPX simulation results obtained from this research show that the maximum surface flux reached the tumor with dimensions of 2×4×4 cm at a fixed depth of 3 cm under the radiation of a point source with a fixed energy of 6 MeV and a spectrum width of 0.6 μm, in the center of the tumor and receiving less surface flux around the tumor is caused by the way of dose distribution. Also, at this level of energy, there is a possibility of various phenomena such as the Bremszhang and Compton effect, but according to the predictions obtained from the code, the template phenomenon in the creation of electrons is the Compton effect. Using the code, it is possible to track a state up to several million particles to analyze the simulation and the obtained answer, and it can be seen that the 6 MeV energy that is used in the Omid Hospital of Isfahan is so low in error that it is necessary. It should be noted that this mode is for the standard and healthy device in terms of quality control. On the other hand, the detection of a higher number of heavy electrons also shows that only a certain amount of particles can enter the tissue, which indicates that the electron weight in the tissue is constant or close to constant, regardless of the number of particles.

ACKNOWLEDGMENT

All the patients who participated in this study are appreciated especially Mrs. Bahare Khaksar Jalali and all researchers at the Laser and Biophotonics Research Center in Biotechnology, Islamic Azad University, Isfahan Branch (Khorasgan).

REFERENCES

[1] R. Khabaz, "Phantom dosimetry and cancer risks estimation undergoing 6 MV photon beam by an Elekta SL-25 linac," Appl. Radiat. Isot. vol. 163, pp. 109232, 2020.

[2] Z. Xu, X. Chen, Z. Sun, C. Li, and B. Jiang, "Recent progress on mitochondrial targeted cancer therapy based on inorganic nanomaterials," Mater. Today Chem. vol. 12, pp. 240–260, 2019.

[3] S. Siddique and J. C. L. Chow, "Artificial intelligence in radiotherapy," Reports Pract. Oncol. Radiother. vol. 25, no. 4, pp. 656–666, 2020.

[4] J. C. L. Chow, "Artificial intelligence in radiotherapy and patient care," in Artificial Intelligence in Medicine, Springer, vol. 95, pp. 1–13, 2021.

[5] J. F. Briesmeister, "MCNPTM-A general Monte Carlo N-particle transport code," Version 4C, LA-13709-M, Los Alamos Natl. Lab. 2000.

[6] I. G Evseev, H. R Schelin, S. A Paschuk, E. Milhoretto, J. A P Setti, O. Yevseyeva, J. T de Assis, J. M Hormaza, K. S Díaz, and R. T Lopes, "Comparison of SRIM, MCNPX and GEANT simulations with experimental data for thick Al absorbers," Appl. Radiat. Isot. vol. 68, no. 4–5, pp. 948–950, 2010.

[7] M. Mirzaie, A. A. Mowlavi, S. Mohammadi, and H. Mirshekarpour, "Absorbed dose calculation from beta and gamma rays of 131I in ellipsoidal thyroid and other organs of neck with MCNPX code," ISMJ, vol. 15, pp. 201–208, 2012.

[8] N. Azadegan, M. Hassanpour, M. U. Khandaker, M. R. I. Faruque, K. S. Al-mugren, and D. A. Bradley, "Calculation of secondary radiation absorbed doses due to the proton therapy on breast cancer using MCNPX code," Radiat. Phys. Chem. vol. 183, pp. 109427, 2021.

[9] X. G. Xu and K. F. Eckerman, *Handbook of anatomical models for radiation dosimetry*, CRC Press, 2009.

[10] U. Javaid, K. Souris, S. Huang, and J. A. Lee, "Denoising proton therapy Monte Carlo dose distributions in multiple tumor sites: A comparative neural networks architecture study," Phys. Medica, vol. 89, pp. 93–103, 2021.

[11] N. Reynaert, S.C. van der Marck, D.R. Schaart, W. Van der Zee, C. Van Vliet-Vroegindeweij, M. Tomsej, J. Jansen, B. Heijmen, M. Coghe, and C. De Wagter, "Monte Carlo treatment planning for photon and electron beams," Radiat. Phys. Chem. vol. 76, pp. 643–686, 2007.

[12] D. Sarrut, M. Bardiès, N. Boussion, N. Freud, S. Jan, Jean Michel Létang, G. Loudos, L. Maigne, S. Marcatili, T. Mauxion, P. Papadimitroulas, Y. Perrot, U. Pietrzyk, C. Robert Robert, D. R. Schaart, D. Visvikis, and I. Buvat , "A review of the use and potential of the GATE Monte Carlo simulation code for radiation therapy and dosimetry applications," Med. Phys. vol. 41, pp. 64301(1-14), 2014.

THIS PAGE IS INTENTIONALLY LEFT BLANK.